Ocean Dynamics (2014) 64:315–324
DOI 10.1007/s10236-013-0683-4

Untangling spatial and temporal trends in the variability of the Black Sea Cold Intermediate Layer and mixed Layer Depth using the DIVA detrending procedure

A. Capet · C. Troupin · J. Carstensen · M. Grégoire · J.-M. Beckers

Received: 11 June 2013 / Accepted: 17 December 2013 / Published online: 26 January 2014

Abstract Current spatial interpolation products may be biased by uneven distribution of measurements in time. This manuscript presents a detrending method that recognizes and eliminates this bias. The method estimates temporal trend components in addition to the spatial structure and has been implemented within the Data Interpolating Variational Analysis (DIVA) analysis tool. The assets of this new detrending method are illustrated by producing monthly and annual climatologies of two vertical properties of the Black Sea while recognizing their seasonal and interannual variabilities : the mixed layer depth and the cold content of its cold intermediate layer (CIL). The temporal trends, given as by-products of the method, are used to analyze the seasonal and interannual variability of these variables over the past decades (1955–2011). In particular, the CIL interannual variability is related to the cumulated winter air temperature anomalies, explaining 88 % of its variation.

Keywords Black Sea · Data interpolation · Detrending · Inverse method · 40°N–48°N · 27°E–42°E · Cold intermediate layer · Mixed layer depth · Climatologies

Responsible Editor: Emil Vassilev Stanev

Electronic supplementary material The online version of this article (doi:10.1007/s10236-013-0683-4) contains supplementary material, which is available to authorized users.

A. Capet (✉) · J.-M. Beckers
Department of Astrophysics, Geophysics and Oceanography (AGO), GeoHydrodynamics and Environment Research (GHER), Université de Liège, Allée du 6-Août, 17, Sart-Tilman B5a, 4000 Liège, Belgium
e-mail: arthurcapet@gmail.com

C. Troupin
TMOOS Department, IMEDEA (CSIC-UIB), Esporles, Balearic Islands, Spain

J. Carstensen
Department of Bioscience, Aarhus University, Frederiksborgvej 399, 4000 Roskilde, Denmark

M. Grégoire
Department of Biology, Ecology and Evolution, Oceanology Laboratory, Université de Liège, Allée de la Chimie, 3, Sart-Tilman B6c, 4000 Liège, Belgium

1 Introduction

Climatologies, i.e., average fields interpolated from in situ data gathered over a large period, are widely used in earth sciences. However, monitoring data are typically heterogeneously distributed in time and space, leading in some cases to flawed analysis if this heterogeneity is not adequately accounted for. For instance, if the mean annual temperature field over the Northern Hemisphere is computed with all the available data, the result will overestimate the true mean temperature, since there are more measurements in summer than in winter. Similarly, the mean temperature field will be biased if data from cold and warm years are not equally represented in all regions.

To remedy this impact, which occurs when unavoidable heterogeneous distribution of data is combined with high variability, we present a detrending method (Duchon 1977) that has been implemented in the existing Data Interpolating Variational Analysis (DIVA, Troupin et al. 2012) tool.

The cases of the Black Sea cold intermediate layer (CIL) (e.g., Stanev et al. 2003) and mixed layer depth (MLD) (e.g., Kara et al. 2009) are ideal examples of application since (1) the CIL (resp. MLD) exhibits an important interannual (Oguz et al. 2006) (resp. seasonal) variability and (2) sampling in the Black Sea is characterized by strongly uneven temporal coverage.

The Black Sea is an enclosed basin, characterized by a strong permanent halocline at approximately 150-m depth, which separates the surface layer, receiving substantial freshwater inputs from several large rivers discharging mainly to the northwestern shelf and the deep waters receiving saltwater inflows from the Mediterranean Sea through the Bosphorus. The surface layer is advected by a basin-wide cyclonic current, referred to as the *rim current* and further subdivided in two main gyres (Korotaev et al. 2003), which intensifies in winter and controls the curvature of the halocline (shallower in the center of the basin, deeper in the periphery).

Cold and dense waters are formed in winter, when surface cooling breaks down the summer thermal stratification and the water column above the halocline becomes fully mixed. The convective sinking of the cold surface waters is limited by the permanent halocline because of denser saline water below. This mechanism leads to the formation of a minimum temperature layer located between the halocline (∼100–150 m) and the summer thermocline (∼20–50 m), known as the cold intermediate layer. Stanev et al. (2003) located the main regions of CIL formation: (1) west of the Crimea peninsula, where surface-cooled fresh waters are mixed with underlying saltier waters; and (2) in the central basin where the winter outcropping of the deep isopycnals allow the cooling to penetrate directly to the density levels of the CIL (which is not possible for the northernmost part of the northwestern shelf area where surface cooling is nevertheless stronger).

The detrending method applied in this work provides monthly climatological fields of the MLD and the CIL cold content (CCC), i.e., the temperature anomaly integrated over the CIL vertical extension (Section 3.1.1), while recognizing the impact of their seasonal and interannual variabilities on the data representativity. The trends assigned to each year by the methodology provide long-term time series used to investigate the interannual variability of MLD and CCC and their relationship to atmospheric drivers.

While Oguz et al. (2006) and Capet et al. (2012) showed that the CIL follows the interannual variability of air temperature, Stanev et al. (2003) identified that it is not entirely renewed every year and that the remaining CIL at the end of summer prepares the winter CIL formation for the next year. Also, Piotukh et al. (2011) indicated the preponderant influence of winter mean (rather than annual mean) surface air temperature on the thermohaline characteristics of the cold content for the next summer. This indicates that the Black Sea hydrodynamics, and in particular regarding the CIL, present regular seasonal cycles, and that interannual variability may be perceived as year long persistent anomalies.

The rim current, which derives mostly from the surface wind vorticity (negative curl causes strong rim current), is known to affect the Black Sea vertical structure but its specific impact on the CIL is difficult to appreciate directly because the occurrence of cyclonic wind patterns is correlated to that of cold air temperature (Capet et al. 2012).

The paper is organized as follows: Section 2 provides a short description of DIVA and describes the detrending procedure and its implementation within DIVA. Section 3 presents an application of the detrending methodology on the Black Sea MLD and CCC and an analysis of their temporal trends. The conclusions concerning the Black Sea and general limitations of the method are discussed in Section 4.

2 Data detrending

2.1 The DIVA method

DIVA stands for Data Interpolating Variational Analysis. It is a method used to interpolate spatially inhomogeneously distributed data. The principle of DIVA is to construct an analyzed field φ that satisfies a set of constraints expressed in the form of a cost function over a domain Ω. Typically, in oceanography, Ω is the part of the considered domain covered by the sea. The cost function is made up of (1) an *observation constraint*, which penalizes the misfit between data and analysis; (2) a *smoothness constraint*, which penalizes the irregularity of the analyzed field (gradients, Laplacian, etc.); and (3) a *behavior constraint*, which takes into account physical laws (advection, diffusion, sinks/sources).

In this paper, only the first two constraints will be considered. In the particular case where the observation constraint is much stronger than the smoothness constraint, the results of the minimization of the cost function is a spline interpolation: the analysis has to contain all the data points. Such a solution is not suitable in the case of atmosphere or ocean observations because it does not consider the noise present in the data (measurement errors, but also *representativity* errors). In other words, the estimated field should mimic the observations rather closely, although maintaining a reasonable degree of smoothness to avoid over-fitting the data.

2.1.1 Formulation

Let us assume that we work with data anomalies, i.e., a reference (or background) field is subtracted from the data points prior the analysis. Considering a series of N data anomalies d_i at locations (x_i, y_i), the cost function reads in Cartesian coordinates:

$$J[\varphi] = \int_\Omega \left(\nabla\nabla\varphi : \nabla\nabla\varphi + \alpha_1 \nabla\varphi \cdot \nabla\varphi + \alpha_0 \varphi^2\right) \mathrm{d}\Omega + \sum_{i=1}^{N} \mu_i \left[d_i - \varphi(x_i, y_i)\right]^2 = J_{\mathrm{smooth}}[\varphi] + J_{\mathrm{obs}}[\varphi], \tag{1}$$

where μ_i, α_0 and α_1 are coefficients related to characteristics of the dataset (Section 2.1.2). ∇ is the horizontal gradient operator and $\nabla\nabla\varphi : \nabla\nabla\varphi = \sum_i \sum_j (\partial^2\varphi/\partial x_i \partial x_j)(\partial^2\varphi/\partial x_i \partial x_j)$, the generalization of the scalar product of two vectors.

The first term of (1) measures the spatial variability (curvature, gradient, and value) of the analyzed field and is identified as the smoothness constraint. The penalization of second derivatives is similar to the smoothing spline formulation (e.g., Wahba 1975; Wahba and Wendelberger 1980). The second term is a weighted sum of data analysis misfits and is identified as the observation constraint: it tends to pull the analyzed field towards the observations. The analyzed field $\varphi(x, y)$ is obtained as the balance between observation and smoothness constraints, once the parameters have been determined. Further details about the DIVA interpolation technique are given by Brasseur et al. (1996) and Troupin et al. (2013).

2.1.2 Analysis parameters

By using a nondimensional version of (1), it can be easily shown (e.g., Troupin et al. 2012) that the coefficients of (1) are related to (1) the relative weights w_i attributed to each observation d_i, (2) the correlation length L, and (3) the signal-to-noise ratio λ, according to the following:

$$\alpha_0 = \frac{1}{L^4}, \quad \alpha_1 = \frac{2}{L^2}, \quad \mu_i = \frac{4\pi\lambda w_i}{L^2} \quad \text{with} \quad \sum_{i=1}^{N} \frac{1}{w_i} = N.$$

These relations simply show that knowing L, λ, and w_i allows the determination of the analysis parameters α_0, α_0, and μ_i of the cost function.

Some tools are implemented in DIVA in order to estimate the values of L and λ, based on the data correlations and on generalized cross validation (Brankart and Brasseur 1996; Troupin et al. 2013).

2.1.3 Finite-element solver

The minimization of (1) is solved with a finite-element technique: the domain of interest Ω is covered by a mesh made up of triangular elements (see Fig. 2a), and in each element, the solution φ_e is expanded in terms of connector values, which ensure that the solution is continuously derivable (Brasseur et al. 1996), and shape functions, which serve to compute the field at any desired location.

2.2 Implementation of detrending in DIVA

If we define one group (e.g., the year), each data point is in one and only one class C_j (e.g., 1990, 1991, etc.) of this group. The data analysis misfit term of the functional (1) can be rewritten by including an unknown trend value for each class $(d_{C_1}, d_{C_2}, \ldots)$:

$$J_{\mathrm{obs}}[\varphi] = \sum_{i \in C_1} \mu_i [d_i - d_{C_1} - \varphi(x_i, y_i)]^2 + \sum_{i \in C_2} \mu_i [d_i - d_{C_2} - \varphi(x_i, y_i)]^2 + \ldots \tag{2}$$

If the function $\varphi(x, y)$ were known, minimization with respect to each of the unknowns d_{C_j} would yield

$$d_{C_1} = \frac{\sum_{i \in C_1} \mu_i [d_i - \varphi(x_i, y_i)]}{\sum_{i \in C_1} \mu_i} \tag{3}$$

and similarly for the other classes: the trend for each class is the weighted misfit of the class with respect to the overall analysis. Obviously, the solution φ is not known, since it is actually the result of the minimization process, but this issue is solved by iterating and starting with an analysis without detrending. Using the field φ, we calculate a first guess of the trends in each group and subtract it from the original data. Following this, a new analysis is performed, the trends are recalculated, and the iterations continue until a specified convergence criterion is fulfilled.

The procedure can be generalized with several groups of classes (e.g., year, month, time of the day, etc.); in this case, detrending is applied hierarchically: (1) Trends for the first group are calculated and removed from the data; (2) The second group is treated and so on; (3) Once the data have been detrended, a new DIVA analysis is performed; (4) With the new analysis, the data analysis misfit (or residual) can be reused to improve the trend estimates. The procedure is repeated a predefined number of times, which ensures convergence in all the cases we tested.

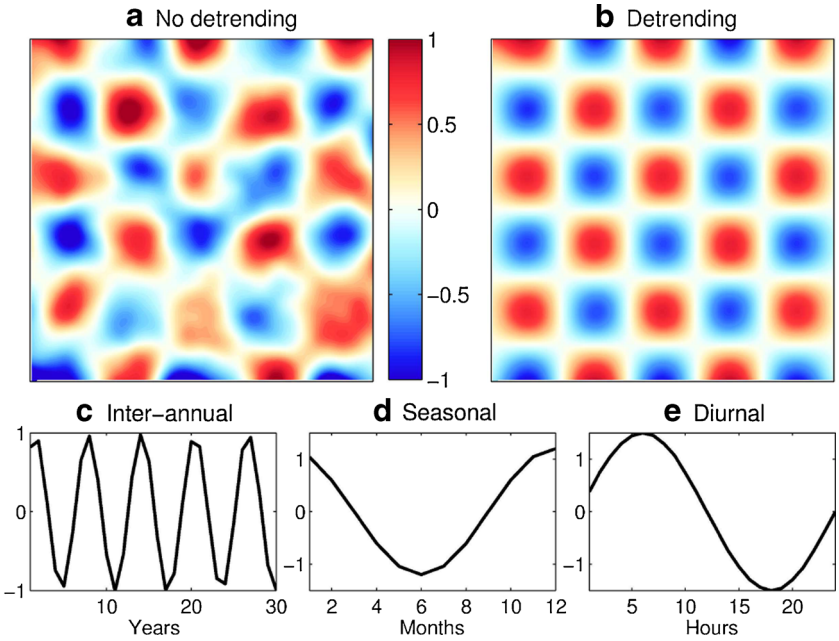

Fig. 1 Example of a reconstruction without detrending (**a**), with detrending (**b**), and the trends obtained from the data (**c**–**e**), where the x-axis indicates the different classes of the three groups. The *color bar* is common to **a** and **b**

2.3 Synthetic example

To illustrate how the detrending helps to reconstruct the spatial distribution of a time-varying variable, we consider the following artificial example: A variable with a fixed and known spatial distribution (a sin-cosine structure) is modulated by a seasonal cycle, a daily cycle, and interannual variations. Samples are taken randomly in space and time and are then used to reconstruct the spatial distribution with DIVA. The results with and without considering detrending are compared.

In this example, the groups considered for the detrending are thus years, months, and hours. The corresponding classes are the discrete values of these (e.g., 0, 1, ..., 23, for the group "hours").

Without detrending, each observation is considered an equal representative of the same static field, disregarding the temporal structure of the data, which amounts to ignore the nonsynoptic character of punctual sampling and results in a flawed analyzed field, dependent on the sampling distribution (Fig. 1a).

When considering the detrending, the periodic structure is perfectly recovered (Fig. 1b). Note that the reconstruction is perfect in this case because the temporal trend is spatially homogeneous.

Along with the detrended spatial analysis, the tool also provides the trend identified for each group (Fig. 1c–e) which may also be of direct scientific interest when the technique is applied to field observations, as shown in the next section.

3 Real-case application: the Black Sea mixed layer depth and cold intermediate layer cold content

3.1 Materials

3.1.1 Data extraction

While interpolation methods are often applied on variables that may be directly measured (e.g., sea temperature, salinity, etc.), these examples address vertical properties derived from vertical profiles: the CCC (e.g., Stanev et al. 2003) and the MLD (Kara et al. 2009).

Profiles of temperature and salinity are obtained from the World Ocean Database (Boyer et al. 2009) in the box 40°–47°30°N, 27°–42°**E** for the period of 1955–2011.

Since the CIL has a minimal depth deeper than 50 m, analysis (interpolation and detrending) are only carried out for the deeper parts of the Black Sea (>50 m). The CCC corresponds to the relative heat deficit in the CIL and is thus expressed negatively in terms of joules per square meter (Piotukh et al. 2011). It is computed as the vertical integral of the temperature anomaly over the vertical extension of the CIL, limited by the $T = T_0$ isotherms and a density criterion ($\rho > 1{,}014$ kg m^{-3}) (Stanev et al. 2003):

$$\mathrm{CCC} = c\rho \int_{\mathrm{CIL}} [T(z) - T_0]dz, \tag{4}$$

where ρ is the density, and c the heat capacity. The value of CCC is set to 0 if the profile covers the usual CIL vertical extent without displaying temperatures lower than T_0. Historically, the value $T_0 = 8$ °C has often be used to define

the CIL (Blatov et al. 1984). However, according to recent observations that attest the presence of the CIL layer as a physical phenomenon without temperature below 8 °C, we rather use the value $T_0 = 8.35$ °C recommended by (Stanev et al. 2013). In order to allow an unbiased estimation of the CIL cold content, eligible profiles should (1) contain a minimum of six measurements, (2) contain an upper observation above 30 m, and (3) extend to lower boundary of the CIL (or close to the bottom).

For the MLD, the analysis are performed on the whole Black Sea and Sea of Marmara, while the Azov Sea was excluded from the analysis for lack of data. The MLD is defined as the depth where a density difference $\Delta\rho$ compared to the 3-m depth density reaches a threshold of 0.125 kg m^{-3} as proposed for the Black Sea by Kara et al. (2009). Eligible profiles for the MLD should (1) contain a minimum of four measurements, (2) contain an upper observation above a 3-m depth, and (3) present a density difference bigger than 0.125 kg m^{-3}.

3.1.2 Data distribution

The monthly distribution of data is heterogeneous, with a minimum of 892 selected profiles in January and a maximum of 3,131 in May. The winter-summer imbalance is evident: the July–September period has 60 % more profiles than in the January–March period. The interannual data distribution is also quite irregular with a majority (59 %) of profiles between 1982 and 1995.

While the spatial coverage is sufficient for the considered analysis, selected profiles are generally more concentrated close to the coast than in the central basin and are more numerous in the western basin than in the eastern part (profile locations are shown for March in Figs. 2 and 3 and for all months in the Supporting Material).

3.1.3 Data weighting

In order to reduce the influence of specific missions with a large number of profiles concentrated in a small area and within a relatively short period, a different weight w_i (Section 2.1.2) is applied on each data point, according to

$$w_i = 1/N_i,$$

with N_i as the number of measurements within the same month and same year and within a 0.2° radius around the i^{th} data point.

3.1.4 Atmospheric predictors

Meteorological time series used to analyze the CIL interannual trend are constructed from the ERA-40 (1958–2000; 1.125° resolution) and ERA-interim (1980–2012; 0.75° resolution) reanalysis, provided by the European Center for Medium-Range Weather (ECMWF) data server. The 1958–2012 merged time series are constructed by unbiasing the distinct datasets in order to equal the distinct averages over the overlapping period (1980–2000). The time series constructed as potential predictors concern winter (December–March) and summer (May–September) air temperature and wind curl anomalies. For a given year (e.g., 1994), T_w refers to the winter temperature of this year (December 1993 to March 1994), while T_{w-1} refers to that of the previous year (December 1992 to March 1993), and so on.

3.2 Results

3.2.1 Climatologies

Annual and monthly climatologies for CCC and MLD may be found in the Supporting Online Material, both as pictures and NetCDF files. These climatologies are suitable for further use (e.g., in modeling studies) and benefit from the general assets of the DIVA interpolation methods (Troupin et al. 2012, 2013). For instance, previous MLD climatologies presented by Kara et al. (2009) does not account for the presence of coast during spatial interpolation, resulting in a contamination of the Black Sea field from profiles issued from the Marmara Sea. In the following, we focus on a few selected analysis to illustrate specific issues of the DIVA detrending tool.

Consistently with the current knowledge on the Black Sea circulation, the annual MLD climatology (Fig. 3) reveals deeper mixed layer on the periphery of the central basin. Stronger mixing appears clearly all along the shelf break, from the Crimea Peninsula, where the region of convective CIL formation is well marked, to the Bosphorus entrance. On the northwestern shelf, the freshwater input maintains a shallow mixed layer in the vicinity of the river mouths.

The CCC climatologies indicates a region of persistence of the CIL layer located west of the Crimea Peninsula, between the shelf slope and the rim current. During summer, high cold content is maintained along the southern peripheral region, where recurrent anticyclonic eddies between the coast and the rim current induce a deep halocline level (∼110–140 m) which gives space for the CIL well below the warm surface waters. This is particularly visible in the south-eastern region of the strong semipermanent Batumi eddy (e.g., Korotaev et al. 2003). The ratio between CCC in the Rim current zone and the central part is in agreement with the ratio [1.5–2.5] given by Piotukh et al. (2011).

3.2.2 Effects of the detrending on the analysis

The magnitude of the CCC interannual variability is slightly higher than that of its seasonal variability. The majority of data has been collected during the period between 1985 and 1995 which was a "cold" period characterized by low air temperature and high CIL cold content (Oguz et al. 2006; Piotukh et al. 2011; Capet et al. 2012). Because of this distribution, a classic analysis without detrending gives more weight to these years, which results in a bias towards high cold content in the annual and monthly climatologies, not representative of the averaged situation for the period of 1955–2011. The detrending procedure corrects this bias as illustrated by the comparison of Fig. 2b, c and Fig. 2e, f, showing the annual and monthly climatology for March (see Supporting Online Material for the others months) obtained with and without detrending. It is also worth mentioning that without detrending, localized CIL minima are introduced to the climatologies: these are artifacts resulting from irregular data distribution across years and are eliminated with the detrending method.

In the case of the MLD, seasonal variability is higher than interannual variability. This example thus illustrates the bias introduced this time by the uneven seasonal distribution of the original data. As more data are available in summer time, when the MLD is small, the classical analysis results in annual climatology fields biased towards small MLD values,which is corrected by the detrended analysis (Fig. 3b, c). Because of the low interannual variability, with respect to the seasonal variability, the detrending method does not impact much on the monthly climatologies.

3.2.3 Interpretation of the trends

As a by-product of the climatologies, DIVA provides the trends assigned to each month and each year. The trend corresponding to one class (e.g., a given year) corresponds to the averaged misfit of the data of this class with respect to the overall analysis. Obviously, these temporal trends still bear some representativity error due to the spatial distribution of data, but this error is minimized by the detrending procedure by comparison with the trends that would obtained from the anomalies with respect to a basin-wide average. In order to consider realistic values rather than anomalies, the time series referred to as "trends" in the following and depicted in Figures 4 and 5 are obtained by adding the average value of the annual analysis to the trends initially provided by DIVA. Compared to the time series constructed by simply averaging the data within each year, the present interannual trend allows a better consideration of (1) uneven spatial distribution, because they rely on the misfit with the climatological analysis rather than on the absolute values, hence consider the spatial variability; and (2) uneven seasonal distribution, because seasonal trends are identified simultaneously, during the same iterative procedure. The temporal trends derived from the analysis are therefore appropriate to study on the temporal dynamics of the analyzed variable.

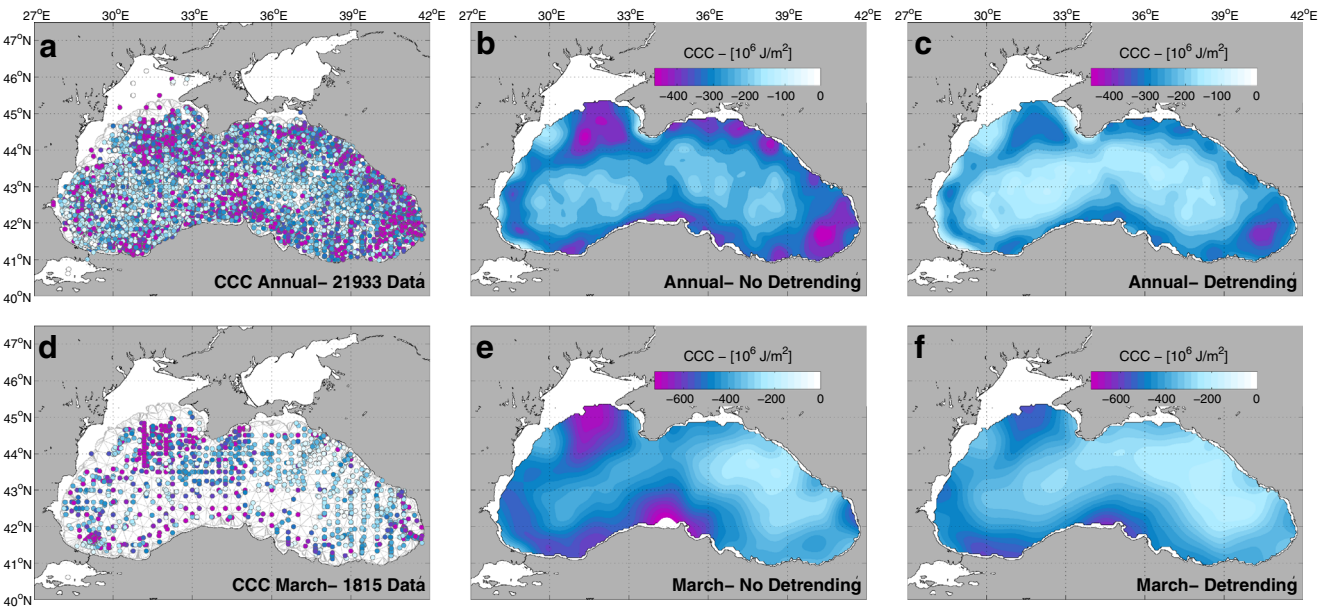

Fig. 2 Cold content of the Black Sea CIL. **a** Values obtained from the vertical profiles and annual climatologies interpolated using DIVA **b** without and **c** with detrending. **d** Values obtained from the vertical profiles for March and monthly climatologies interpolated using DIVA **e** without and **f** with detrending

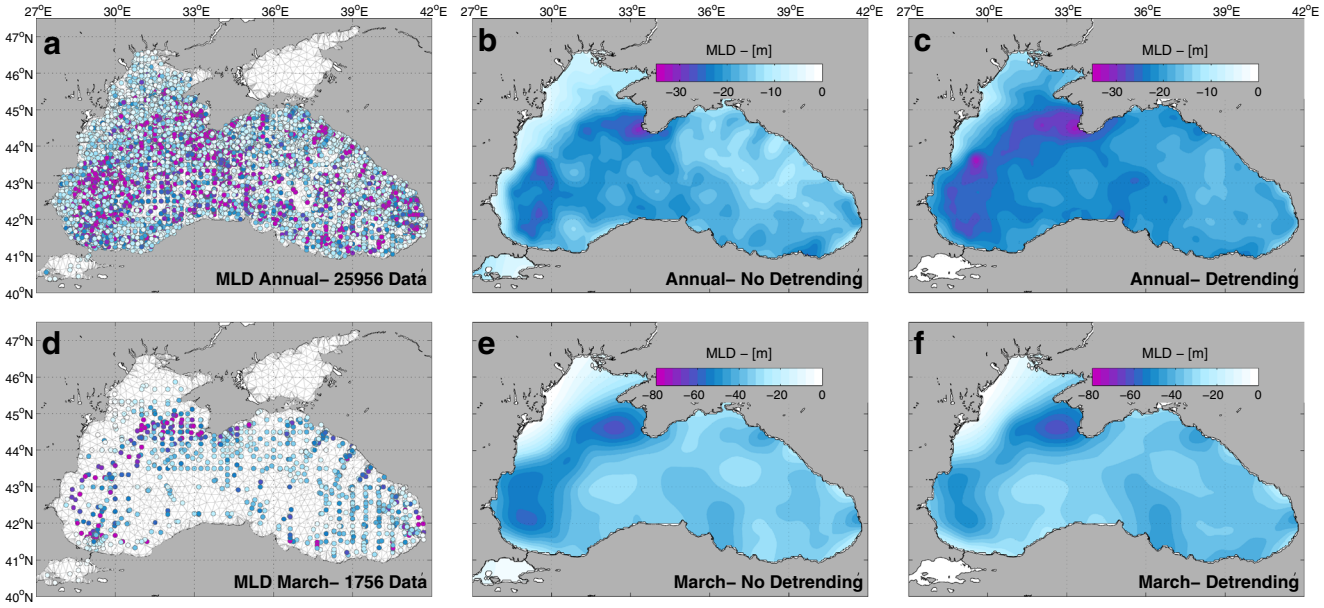

Fig. 3 Mixed layer depth. **a** Values obtained from the vertical profiles and annual climatologies interpolated using DIVA **b** without and **c** with detrending. **d** Values obtained from the vertical profiles for March and monthly climatologies interpolated using DIVA **e** without and **f** with detrending

In the following, we use the trends to compare the range of seasonal and interannual variability of CCC and MLD and assess whether systematic relationships between the interannual trends and atmospheric conditions may be identified.

The seasonal trend is very clear in the case of MLD (Fig. 4b), revealing the stronger mixing in February, the sharp onset of the thermocline from March to May, and the slower deepening of the mixed layer from August to February.

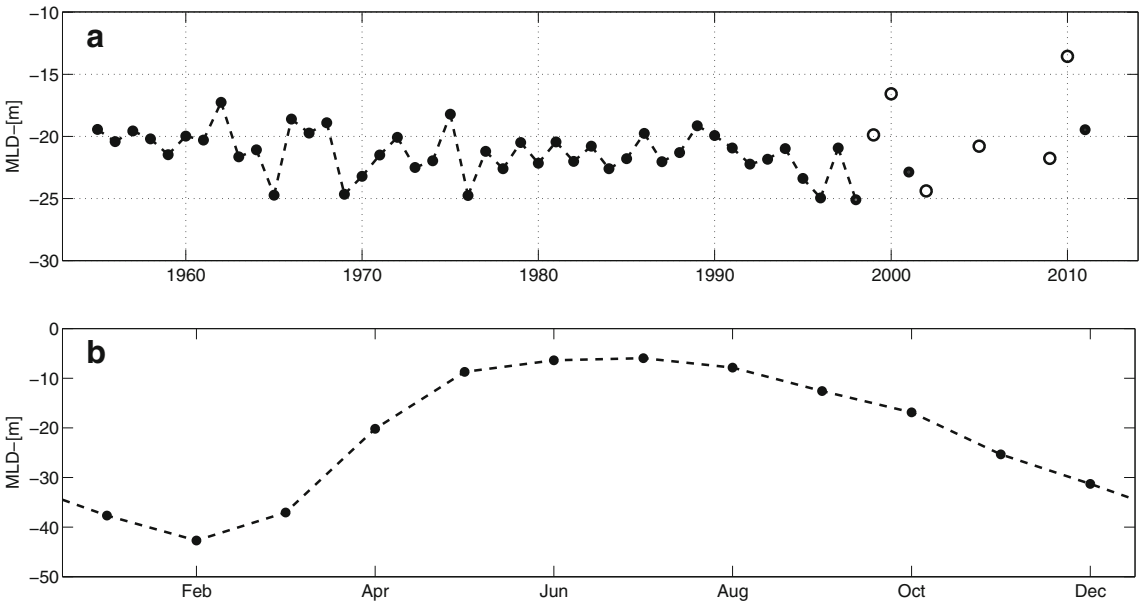

Fig. 4 **a** Interannual variability of the mixed layer depth as identified by the DIVA detrending tool over the period of 1955–2011, (*filled circles*, years with more than 50 eligible profiles; *empty circles*, years with more than 25 and less than 50 eligible profiles). No significant relationship between the annual anomalies and atmospheric predictors may be derived. **b** Climatological seasonal cycle reconstructed by DIVA with detrending

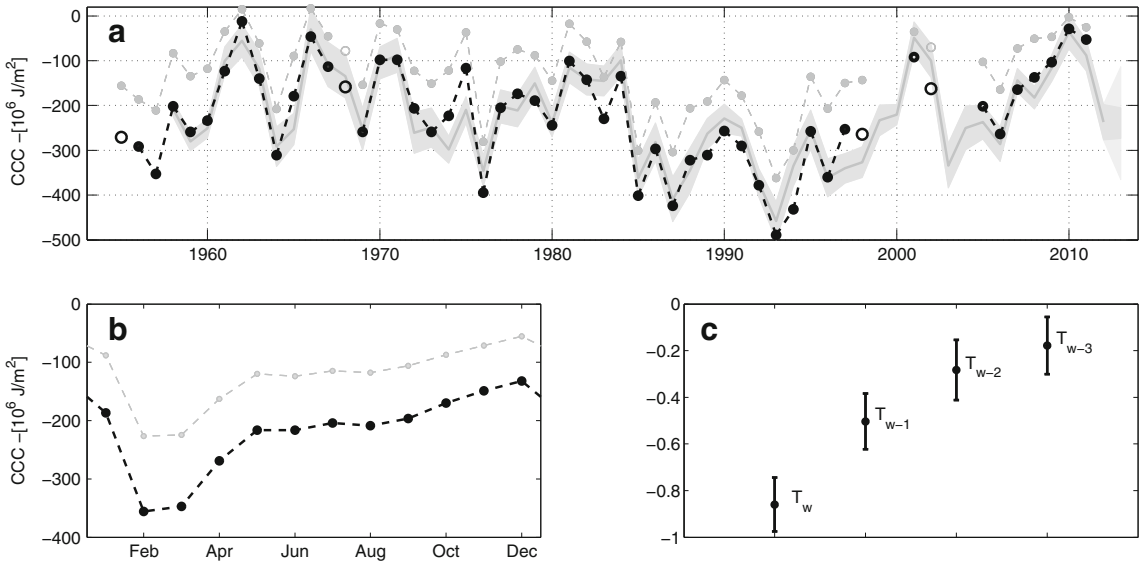

Fig. 5 **a** Interannual variability of the CIL cold content as identified by the DIVA detrending tool over the period of 1955–2011 (*black circles* and *dotted lines*) and predicted by a stepwise regression model (*plain gray line*; the *shaded area* represents the confidence bounds, $p < 0.01$) using the cumulated anomalies of winter air temperature as predictors. Only the years with more than 50 eligible profiles are considered to compute the regression coefficients (*filled circles*); other years containing more than 25 profiles are also indicated (*empty circles*). The explanatory power of past anomalies allows one to infer prediction for the 2013 CIL cold content, assuming average ± 1 standard deviation for the unknown T_w value in 2013. **b** climatological seasonal cycle reconstructed by DIVA with detrending. **c** Standardized coefficients of the selected predictors: central value, $p < 0.05$ confidence intervals. To allow the comparison with previous works, we indicated on panels **a** and **b** the results obtained by using the historical definition $T_0 = 8°\mathrm{C}$ (*gray circles* and *dotted lines*)

The seasonal trend of the CCC (Fig. 5b) indicates the formation season from December to March, and then a first decrease until May when surface warming erodes the upper layer of the CIL, and then another decrease starting from August when the MLD starts to deepen.

No systematic relationships between the interannual trend of MLD and the selected atmospheric predictors could be identified. This indicates that other factors influence this fast responding dynamic (e.g., wind stress). On the large scale, the interannual trend of MLD (Fig. 4a) depicts a slow deepening from the 1960s to mid-1990s, and presumably a shallowing afterwards, but the latter is hindered by the lack of data for the last decade. This long-term tendency, also visible in the case of CCC (Fig. 5a), is in agreement with the long-term influence of North Atlantic Oscillation on the sea surface temperature (Oguz et al. 2006; Capet et al. 2012).

The inertial dynamic of the CIL cold content results in a more coherent signal of interannual variability. In that case, a stepwise regression procedure could be used to express the signal as a response to the atmospheric predictors.

We found that 4 years of winter temperature anomaly was significant ($p < 0.05$) in describing the CIL variability, explaining together 88 % of the signal obtained from the detrending procedure (Fig. 5a). Summer and wind curl predictors were discarded as nonsignificant by the stepwise regression procedure. The preponderance of winter predictors over summer predictors confirms the results of (Piotukh et al. 2011).

The decreasing standardized coefficients (-0.86, -0.50, -0.28, and -0.18 for T_w, T_{w-1}, T_{w-2}, and T_{w-3}, respectively; Fig. 5c) reflect the decreasing influence of past winter air temperature anomalies.

Using predictors from past years only (T_{w-1}, T_{w-2}, T_{w-3}) explains 20 % of the CIL variability, thus giving a partial prediction ability, which was used to infer a prediction interval for the year 2013 by considering the range of average ± 1 standard deviation for T_w for the unknown 2013 winter air temperature.

4 Conclusions

A detrending tool is integrated in the DIVA spatial interpolation tool to correct climatology analysis from the bias caused by uneven temporal sampling over a period with substantial temporal variability.

DIVA is applied to the mapping of the mixed layer depth and cold content of the Black Sea CIL. These properties are derived from the vertical profiles available for the period of 1955–2011. The comparison of the reconstructed fields obtained with and without detrending illustrates the ability

of the method to rectify the monthly climatologies from the bias caused by a higher availability of profiles during the cold 1985–1995 period (CCC example), and the annual climatologies from the bias caused by a higher availability of profiles during the summer period (MLD example).

Moreover, the detrending procedure provides the user with the temporal trends identified to unbias the spatial analysis. These trends may be used to analyze the temporal variability of the considered variable.

As an example, the information on the interannual variability of the cold content of the Black Sea CIL is exploited to evidence, through a stepwise regression analysis, the cumulative effect of air temperature anomaly. Considered jointly, the winter air temperature anomalies of the four past years explain significantly ($p < 0.05$) up to 88 % of the CCC interannual signal. Moreover, the inertial dynamic of the CIL results in a part of explicative power from the past predictors (i.e., air temperature anomalies of the previous years), which gives a partial (20 %) predictive ability concerning the CIL intensity for the year to come.

The chosen example demonstrated the effect of the most apparent representativity error: the one issued from the seasonal and interannual variability, but the same method could be used for other sources of representativity errors (e.g., diurnal variability, different instruments or protocols, different databases, and different observation depths).

In the same way that spatial analysis are corrected from uneven temporal distribution, the temporal trends are partly corrected from the influences of spatial uneven distribution as these are reconstructed from the anomalies between data and the spatial analysis rather than from the anomalies between data and a basin-wide average (see for instance the discussion in Piotukh et al. (2011) concering the CCC case). In its present form, however, the detrending procedure still identifies trends which are considered as uniform over the entire spatial analysis domain. This assumption should be carefully considered for large domains where temporal variability may differ across subregions. For instance, in a domain that encompasses the equator and mid-latitudes, the seasonal trend that will be removed is likely to be too strong for the equatorial region and too weak for temperate latitudes.

Also, the different trends (e.g., seasonal, interannual) are considered to be independent and additive. While this constitutes a valid first approximation, it may be expected that seasonal variations between contrasting years differ in reality by more than a simple constant. Extensive analysis, exploiting the interannual trend to identify contrasting periods, may consider partitioned datasets to evaluate the consistency of the overall seasonal trend during these subperiods.

The relevance of climatological analysis computed over large period affected by temporal variability is a general question that has to be considered specifically for each application. Appropriately, the detrending tool presented in this study provides, along with the climatological product, the additional temporal information needed to address this question.

Acknowledgments The authors thank the European Center for Medium-Range Weather for providing the reanalysis and the US National Oceanographic Data Center for providing access to in situ data through the World Ocean Database. DIVA has received funding from the European Union Seventh Framework Program (FP7/2007–2013) under grant agreement no. 283607, SeaDataNet 2, and from project EMODNET (MARE/2008/03 - Lot 3 Chemistry - SI2.531432) from the Directorate-General for Maritime Affairs and Fisheries. This research was supported by the SESAME Project (EC contract no. GOCE036949) and the PERSEUS Project (EC grant agreement no. 287600). This is a MARE publication.

References

Blatov A, Bulgakov N, Ivanov V, Kosarev A, Tujilkin V (1984) Variability of hydrophysical fields in the Black Sea. Gidrometeoizdat, Leningrad

Boyer TP, Antonov JI, Baranova OK, Garcia HE, Johnson DR, Locarnini RA, Mishonov AV, O'Brien TD, Seidov D, Smolyar IV, Zweng MM (2009) World ocean database 2009, chapter 1: introduction. Tech. rep. US Government Printing Office, Washington. p 216

Brankart JM, Brasseur P (1996) Optimal analysis of in situ data in the Western Mediterranean using statistics and cross-validation. J Atmos Ocean Tech 13:477–491

Brasseur P, Beckers JM, Brankart JM, Schoenauen R (1996) Seasonal temperature and salinity fields in the Mediterranean Sea: climatological analyses of a historical data set. Deep-Sea Res I 43:159–192. doi:10.1016/0967-0637(96)00012-X

Capet A, Barth A, Beckers JM, Grégoire M (2012) Interannual variability of Black Sea's hydrodynamics and connection to atmospheric patterns. Deep-Sea Res II 77–80:128–142. doi:10.1016/j.dsr2.2012.04.010. http://www.sciencedirect.com/science/article/pii/S09670645120\00586

Duchon J (1977) Splines minimizing rotation-invariant semi-norms in Sobolev spaces. In: Schempp W, Zeller K (eds) Constructive theory of functions of several variables. Springer, Berlin, pp 85–100

Kara AB, Helber RW, Boyer TP, Elsner JB (2009) Mixed layer depth in the Aegean, Marmara, Black and Azov Seas: part 1: general features. J Mar Syst 78:S169–S180

Korotaev G, Oguz T, Nikiforov A, Koblinsky C (2003) Seasonal, interannual, and mesoscale variability of the Black Sea upper layer circulation derived from altimeter data. J Geophys Res 108(C4):3122. doi:10.1029/2002JC001508. http://www.agu.org/journals/jc/jc0304/2002JC001508/

Oguz T, Dippner JW, Kaymaz Z (2006) Climatic regulation of the Black Sea hydro-meteorological and ecological properties at interannual-to-decadal time scales. J Mar Syst 60(3–4):235–254. doi:10.1016/j.jmarsys.2005.11.011. http://www.sciencedirect.com/science/article/pii/S092479630500206X

Piotukh VB, Zatsepin AG, Kazmin AS, Yakubenko VG (2011) Impact of the Winter Cooling on the Variability of the Thermohaline

Characteristics of the Active Layer in the Black Sea. Oceanology 51(2):221–230

Stanev E, Bowman M, Peneva E, Staneva J (2003) Control of Black Sea intermediate water mass formation by dynamics and topography: comparison of numerical simulations, surveys and satellite data. J Mar Res 61(1):59–99. doi:10.1357/002224003321586417

Stanev E, He Y, Grayek S, Boetius A (2013) Oxygen dynamics in the black sea as seen by argo profiling floats. Geophys Res Lett 40(12):3085–3090

Troupin C, Sirjacobs D, Rixen M, Brasseur P, Brankart JM, Barth A, Alvera-Azcárate A, Capet A, Ouberdous M, Lenartz F, Toussaint ME, Beckers JM (2012) Generation of analysis and consistent error fields using the Data Interpolating Variational Analysis (DIVA). Ocean Model 52–53:90–101. doi:10.1016/j.ocemod.2012.05.002. http://www.sciencedirect.com/science/article/pii/S14635003120 00790

Troupin C, Ouberdous M, Sirjacobs D, Alvera-Azcárate A, Barth A, Toussaint ME, Beckers JM (2013) DIVA user's guide. GeoHydrodynamics and Environment Research, March edn. http://modb.oce.ulg.ac.be/mediawiki/upload/DIVA/notes/DivaUserGuide_March2013.pdf. Accessed March 2013

Wahba G (1975) Smoothing noisy data with spline functions. Numer Math 24:383–393

Wahba G, Wendelberger J (1980) Some new mathematical methods for variational objective analysis using splines and cross validation. Mon Weather Rev 108:1122–1143